Journal of Solid State Chemistry 230 (2015) 34–41

Contents lists available at ScienceDirect

Journal of Solid State Chemistry

journal homepage: www.elsevier.com/locate/jssc

# Structural study of Ni-substituted $YBaCo_{4-x}Ni_xO_7$ frustrated cobaltites

L.M. Torre [a], G. Aurelio [a,*], E. Granado [b], R.D. Sánchez [a,c]

[a] Consejo Nacional de Investigaciones Científicas y Técnicas, Centro Atómico Bariloche - Comisión Nacional de Energía Atómica, Av. Bustillo 9500, 8400 S. C. de Bariloche, RN, Argentina
[b] Institute of Physics "Gleb Wataghin", University of Campinas - UNICAMP, 13083-970 São Paulo, Brazil
[c] Instituto Balseiro, Universidad Nacional de Cuyo, Av. Bustillo 9500, 8400 S. C. de Bariloche, RN, Argentina

ARTICLE INFO

*Article history:*
Received 18 March 2015
Received in revised form
15 June 2015
Accepted 16 June 2015
Available online 20 June 2015

*Keywords:*
Cobaltites
X-ray powder diffraction
Magnetic frustration

ABSTRACT

In this work we report a study of the thermal stability and the evolution of the crystal structure of Ni-substituted $YBaCo_{4-x}Ni_xO_7$ cobaltites, for $x=0$, 0.10 and 0.20. Synchrotron X-ray powder diffraction and thermodiffraction experiments show that the structural transition $P31c \rightarrow Pbn2_1$, which occurs around room temperature for the parent compound, is shifted up to 40° by the partial substitution Ni-for-Co. Moreover, the transition is shown to be of first order with a volume collapse of $\approx 0.05\%$ and an abrupt contraction of the cell along the *c*-direction. The monoclinic distortion below 100 K reported for the parent compound is also observed in the Ni-substituted samples, suggesting that they also get to order antiferromagnetically below that temperature. Magnetization measurements allowed us to detect a small amount of a ferromagnetic impurity in the sample with $x=0.20$, indicating that the solubility limit of Ni lies below that value. The magnetic susceptibility in the paramagnetic region, as well as the cell parameters in each crystallographic phase, is not significantly modified by these amounts of Ni substitution, in contrast to the marked enhancement of the $P31c$ phase stability upon substitution.


## 1. Introduction

Cobalt oxides have always constituted a focus of interest, due to the wide spectrum of physical properties they exhibit. These properties originate from the very strong interplay among crystal structure, magnetism and electronic transport, giving rise to rich phase diagrams tuned by temperature, pressure, magnetic fields, oxygen content and cationic size. A quite novel member of the cobalt-rich oxides family is the so-called "114-cobaltite" $RBaCo_4O_7$, discovered in 2002 for $R$=Y [1] and later synthesized with $R$=lanthanides and calcium. This compound soon gained attention because it displays two very attractive features. First, it offers the possibility to study frustrated magnetism in the unique topology of a three-dimensional framework of Co tetrahedra in interconnected triangular and Kagomé lattices. Geometric frustration is related to intensively studied phenomena in spin ices and multiferroic materials [2,3], and this compound opens a new possible scenario for its study. A second remarkable property is its capacity of absorption and desorption of gases, which turns these cobaltites outstanding candidates for oxygen-storage and gas-sensors applications [4,5]. They show an extreme affinity for oxygen, being able to uptake up to 1.5 extra atoms per formula unit at 350 °C, and release them again, very abruptly, at 400–450 °C [6–8].

The stoichiometric compound $YBaCo_4O_7$ has a nominal valence for Co of 2.25, so it is assumed that Co is present as $Co^{2+}$ and $Co^{3+}$ in a 3:1 proportion. The structure of this compound is shown in Fig. 1. In its high–temperature form, in the trigonal space group $P31c$, the symmetry imposes a high magnetic frustration. However, it has been shown that for the strictly stoichiometric compound with $\delta=0$, a first–order phase transition to an orthorhombic $Pbn2_1$ space group at a temperature $T_S$ (close to room temperature for $YBaCo_4O_7$ [9,10]) lifts this frustration and allows for the development of a long-range antiferromagnetic (AFM) structure below $T_N \sim 110$ K [9]. The origin and driving force for the structural transition at $T_S$ remain under debate. It was originally suggested that a charge ordering mechanism would occur at $T_S$ [11]; it was also proposed that the transition is driven by the condensation of a phonon mode associated to the rigid-body rotation of the tetrahedra in the Kagomé layers [12]. Finally, Huq et al. [13] proposed that it is driven by a severe under-bonding of $Ba^{2+}$ ions. In Fig. 2 we show the schematic geometrical relation between the unit cells of the $P31c$ and $Pbn2_1$ phases in the $a$–$b$ plane. The lattice parameters are related as $a_O \approx a_T$, $b_O \approx \sqrt{3}a_T$ and $c_O \approx c_T$.

It is interesting to note that the oxygen stoichiometry plays an important role in the trigonal to orthorhombic transition, which is suppressed already for very small values of $\delta$ (as low as 0.02 [14]). A second variable which modifies the transition temperature $T_S$ is the $R$-cation size, as has been shown and discussed by various

* Corresponding author.
*E-mail address:* gaurelio@cab.cnea.gov.ar (G. Aurelio).

http://dx.doi.org/10.1016/j.jssc.2015.06.030
0022-4596/

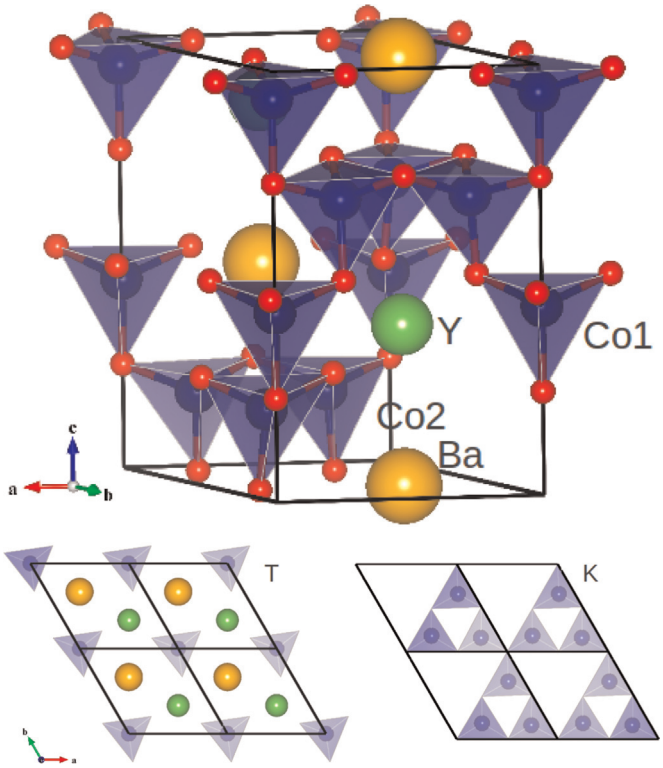


**Fig. 1.** Crystal structure of $YBaCo_4O_7$ above 310 K in the *P*31*c* space group, showing the Co tetrahedra geometry. Labels indicate the different sites. Co1 are located at the triangular layers (T) and Co2 are in the Kagomé layers (K). Bottom: view along the *c*-axis of the T and K layers.

authors [11,15]. Less studied has been the effect on the structural transition of replacing Co with other magnetic ions [16,17]. In this paper, we report a structural study of Ni-doped $YBaCo_4O_7$ cobaltites based on synchrotron X-ray powder diffraction (SXPD).

## 2. Experimental methods

### 2.1. Synthesis

Polycrystalline samples of nominal $YBaCo_4O_7$ (hereafter called Ni-0) and $YBaCo_{4-x}Ni_xO_7$ with $x=0.10$ and 0.20 (alias Ni-10 and Ni-20) were prepared by conventional solid–state reaction. High-purity powders of $Y_2O_3$, $BaCO_3$, $Co_3O_4$ and metallic Ni were thoroughly mixed in an agate mortar at stoichiometric weights. After a de-carbonation process at 1173 K for 12 h, the mixtures were pressed into pellets, annealed during 24 h at 1473 K and slowly cooled at 1 K/min in the furnace. The compression and annealing at 1473 K in air were repeated after re-grinding. Sample Ni-0 was quenched from 1473 K to L-$N_2$ to obtain the stoichiometric compound. The samples containing Ni were cooled inside the furnace at 1 K/min and their precise oxygen stoichiometry was later adjusted by a treatment at 823 K followed by a slow cooling under He flow inside a thermobalance. Samples were checked for impurities using laboratory XRD. Sample Ni-0 was found to contain very small amounts of $Y_2O_3$ and CoO, whereas samples Ni-10 and Ni-20 showed no impurity phases within the detection limit of such technique. In particular, none of the Ni-substituted samples showed any evidence of Ni-based compounds' segregation.

### 2.2. Thermogravimetry

The oxygen uptake and release of $YBaCo_4O_7$ and related compounds have been widely investigated in the literature [6,7,18,14]. It is well established that even small deviations from the precise stoichiometry ($\delta \geq 0.018$) have profound effects on the crystal structure and magnetism of the system [14]. For such reasons, the final oxygen content in our samples was fine-tuned and controlled using TGA (thermogravimetric analysis). The as-synthesized pellets were crushed into smaller pieces of less than 250 mg. Measurements were carried under He flow (50 ml/min at 1000 Torr). Samples were heated from room temperature to 823 K at 5 K/min, then cooled back to room temperature (1st cycle) and the process was repeated (2nd cycle). For data treatment, the initial mass was selected just above 400 K (after any possible loss of water) and the mass loss was computed with respect to this value, after a baseline subtraction.

### 2.3. Synchrotron X-ray powder diffraction

In situ SXPD measurements were performed on the D10B-XPD beamline of the Brazilian Synchrotron Light Laboratory, LNLS, Campinas. An X-ray beam with a wavelength of ~1.0335 Å in a high-resolution configuration using a crystal analyzer was chosen to detect subtle differences between different space groups. The SXPD measurements were performed using copper sample holders with flat-plate shape in reflection geometry, placed inside a cryostat. X-ray diffractograms were recorded in situ between 300 K and 10 K at selected temperatures with a $2\theta$ angular step of 0.005° and 10,000 monitor counts per step. Samples for the SXPD experiment were sieved using a 10 μm mesh in order to reduce crystallite size, increasing the number of crystallites in Bragg condition and their randomness. Nevertheless, the 10 μm mesh

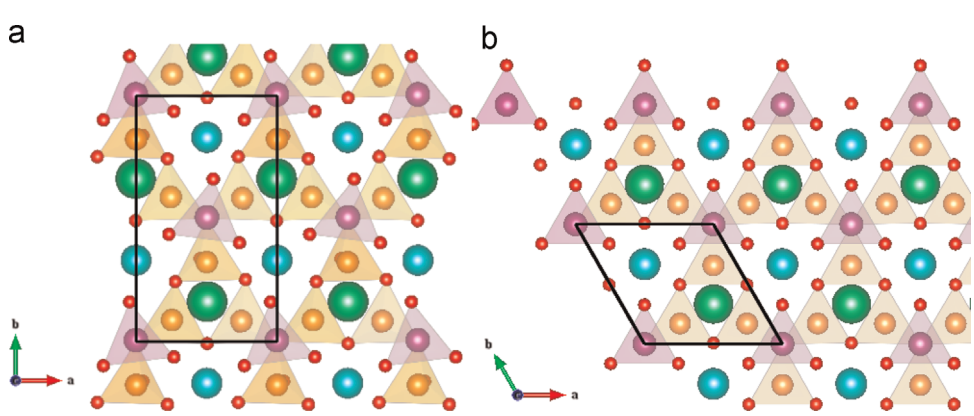


**Fig. 2.** View along *c* of the *P*31*c* (a) and *Pbn*2$_1$ (b) phases of $YBaCo_4O_7$ showing the geometrical relation between them. Only one half of the planes along *c* are projected for simplicity. Co atoms in the triangular and Kagomé layers are represented using different colors only as a guide. (For interpretation of the references to color in this figure caption, the reader is referred to the web version of this paper.)

resulted insufficient to overcome this problem completely and there was no possibility of sample rotation inside the cryostat. For this reason the data were not analyzed using the Rietveld method, instead we used the Le Bail method implemented in FULLPROF [19] to obtain accurate lattice parameters and to follow phase transitions as a function of temperature. Laboratory XPD scans were run on the Ni-0 sample using a high-temperature chamber in a PANalytical Empyrean diffractometer using Cu $K_\alpha$ radiation. Data were collected between $10° < 2\theta < 90°$ with a step of 0.02° and a total counting time of 90 min at 303 K and 333 K.

### 2.4. Magnetization

DC magnetization measurements were performed using a SQUID magnetometer (Quantum Design) between $5\ K < T < 350\ K$ under an applied magnetic field of 1000 Oe, using a warming/cooling rate of 2 K/min. Room temperature hysteresis cycles between $-10\ kOe < H < 10\ kOe$ were collected in a LakeShore vibrating sample magnetometer using the same samples and sample-holders. Data were corrected in both cases by the diamagnetism of the sample holder.

## 3. Results

### 3.1. Oxygen stoichiometry

The TGA measurements show that when heating the samples for the first time after their synthesis, those that had been slowly cooled from 1473 K during the synthesis present a loss of mass occurring between 473 and 523 K, as shown for sample Ni-10 in Fig. 3(b) and for Ni-20 in Fig. 3(c). This behavior is in very good agreement with that reported for the parent compound ($x=0$) in Ar or N2 flow [6,7,18,14]. This mass loss is related to the release of oxygen in excess from the stoichiometric $\delta=0$ value. On the other hand, sample Ni-0 which had been rapidly quenched from 1473 K showed no variation of mass within experimental error (Fig. 3(a)), proving that the quenching process already provides stoichiometric samples. Under the hypothesis that the samples reach the value $\delta=0$ above 723 K, the initial oxygen excess can be computed leading to values between $0.15 \le \delta \le 0.22$ as indicated on the right-hand axes of Fig. 3. The second cycle of heating and cooling confirms that once the $\delta=0$ value is reached, the sample remains stable at $\delta=0$ when cooled in an inert atmosphere. In the following, all the results presented correspond to samples with a $\delta=0$ stoichiometry.

### 3.2. Trigonal to orthorhombic transition

It is well-established in the literature that the parent compound $YBaCo_4O_7$ exhibits a structural transition to the orthorhombic $Pbn2_1$ space group below 313 K [9], whereas Caignaert et al. [10] reported a $T_S$ between 300 K and 310 K. Being a first-order transition [12,13,20], it is characterized by a thermal hysteresis which strongly depends on the kinetics of the experimental technique used for its determination [21]. In any case, precisely at room temperature the parent compound is likely to be in a two-phase state where the $P31c$ (T phase) and $Pbn2_1$ (O phase) are coexisting. In fact, the Rietveld refinements of laboratory XRD data yield better agreement factors for a two-phase mixture in samples Ni-0 and Ni-10. Quite notably, almost none of the papers reporting XRD data at room temperature for the $YBaCo_4O_{7.00}$ compound have considered this issue, even when the lattice parameters reported seem to be the average of those corresponding to each of the structures, as it will become clearer in the remaining discussion.

To explore the phase transition and the effect of Ni-substitution

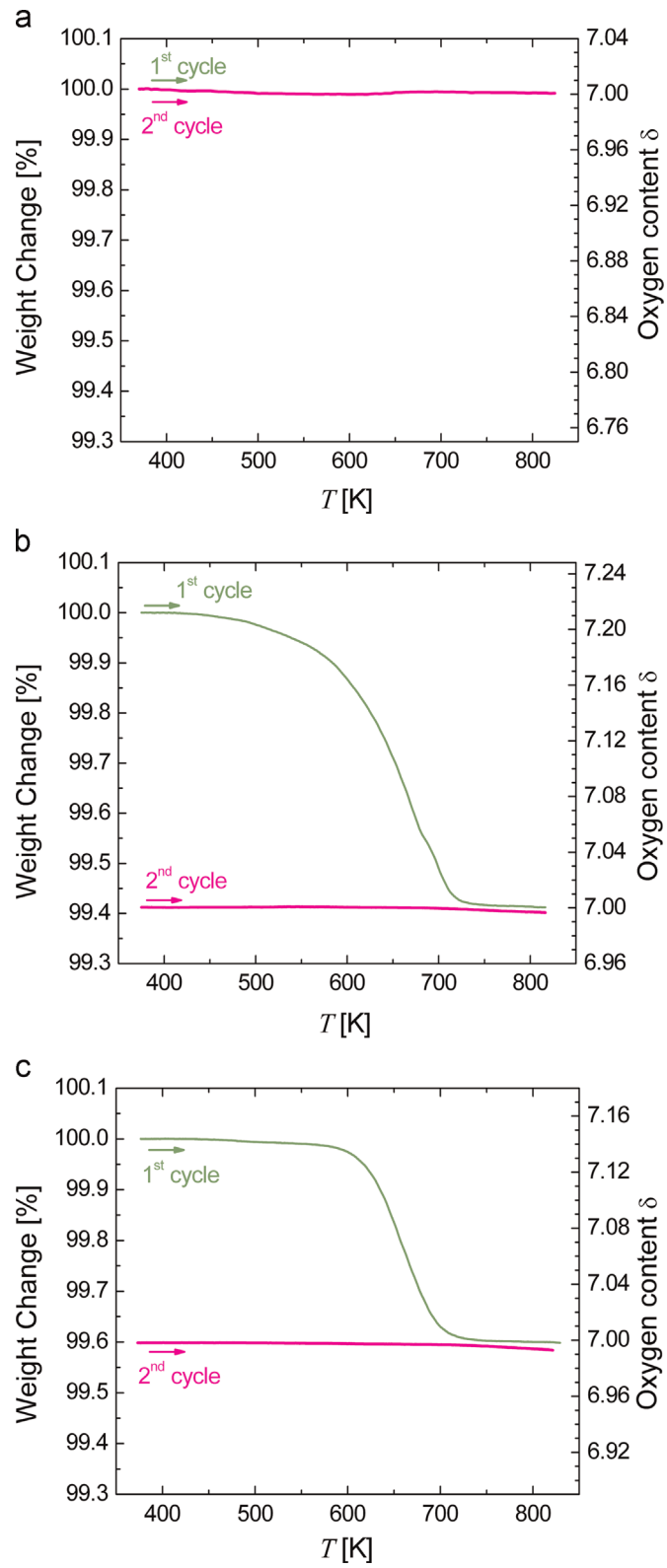


**Fig. 3.** TGA data during two consecutive heating/cooling cycles from 300 K to 823 K for samples Ni-0 (a) previously quenched from 1473 K, and for samples Ni-10 (b) and Ni-20 (c) which had been slowly cooled inside the furnace during synthesis. The experiment was conducted under He flow. The left axes indicate the mass loss whereas the right axes show the evolution of the oxygen non-stoichiometry.

we performed in situ SXPD focusing on selected regions of the scattering angle $2\theta$. In Fig. 4 we present the evolution of the diffractograms of sample Ni-10 upon cooling from 300 K to 270 K.

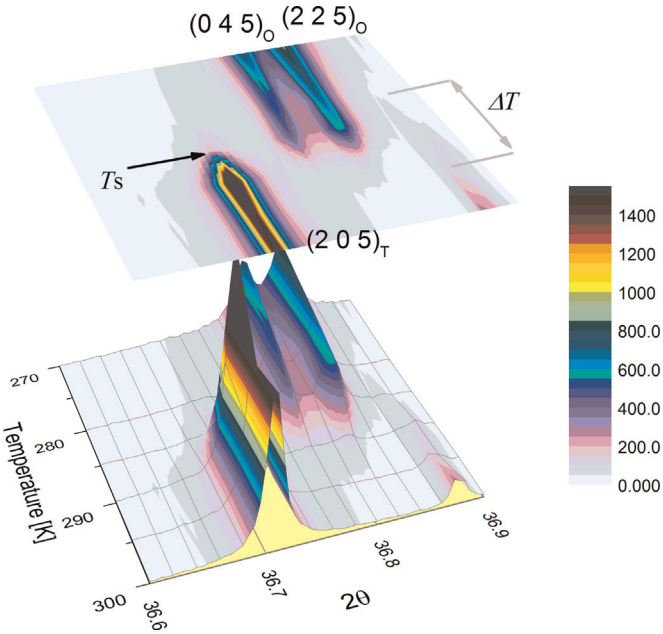


**Fig. 4.** Thermal evolution of diffractograms for a sample $YBaCo_{3.9}Ni_{0.1}O_{7.00}$ collected on cooling at the LNLS synchrotron source. The Bragg reflections were indexed in the *P*31*c* and *Pbn*2$_1$ space groups above and below the transition temperature $T_S$, indicated with an arrow. The region of coexistence of both phases is indicated as $\Delta T$.

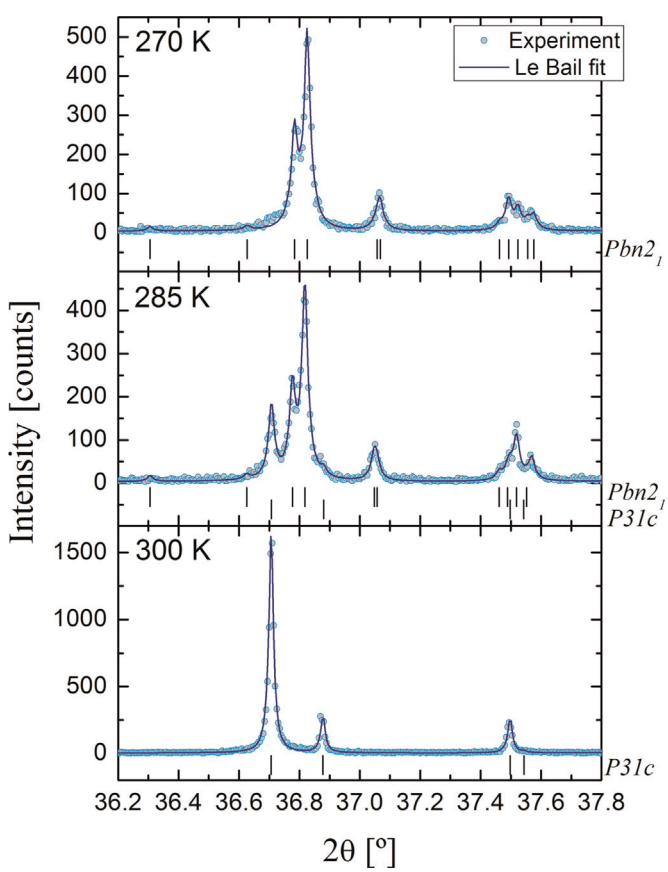


**Fig. 5.** Le Bail fits (solid lines) for the sample $YBaCo_{3.9}Ni_{0.1}O_{7.00}$ at 270 K, 285 K and 300 K. Symbols correspond to the experimental data collected at LNLS on warming from low temperature. The vertical ticks at the bottom represent the Bragg reflections of the *P*31*c* and *Pbn*2$_1$ space groups.

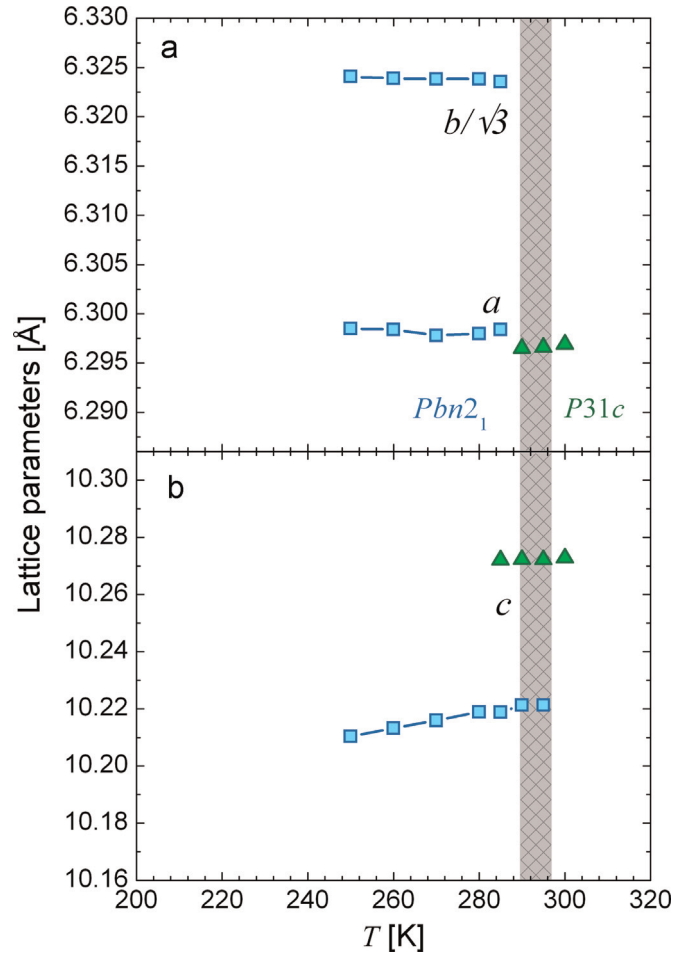


**Fig. 6.** Thermal evolution of lattice parameters $a$, $b/\sqrt{3}$ (a) and $c$ (b) in the *Pbn*2$_1$ and *P*31*c* phases for a sample $YBaCo_{3.9}Ni_{0.1}O_{7.00}$ (from data collected on cooling). The shadowed region represents the coexistence of phases *Pbn*2$_1$ and *P*31*c*.

The cooling rate was of 10°/min. However, each temperature was stabilized before data collection and each measurement took around 2 h. The transition from *P*31*c* to *Pbn*2$_1$ is very well-resolved despite the variations in intensity of the Bragg reflections, which are due to limited grain statistics (see Section 2.3). The transition temperature may be defined as indicated in the graph. However, there is a large temperature range (of at least 10 K) in which the two phases coexist. This range has been indicated with $\Delta T$ in the graph, but we recall that its value will depend on the kinetics of the experiment. To illustrate these results, we present in Fig. 5 the Le Bail fits at three different temperatures for sample Ni-10. At 270 K the sample is in the O phase, and at 300 K the transition to the T phase is already complete. However, the intermediate temperature 285 K shows clearly the coexistence of both O and T phases, indicated by the vertical bars (Bragg reflections) at the bottom of the diffractograms.

From a Le Bail fit in the range $32.5° < 2\theta < 40.0°$ we obtained the lattice parameters as a function of temperature, as shown in Fig. 6. A remarkable discontinuity is revealed across the $T_S$, which reaches a difference of 0.05 Å in the $c$ lattice constant. This behavior is completely different to the one reported by Rykhov et al. [12] for the Lu-114 cobaltite, but instead agrees with the one observed by Maignan et al. [21] in Tm-114 at 175 K. It is interesting to note that in the initial stages of formation of one phase in the other, the lattice seems to be distorted to reduce mismatch, but a few degrees later the two-phase mixture already shows well-resolved differences in lattice parameters, as shown in Fig. 4 for one set of reflections. This abrupt

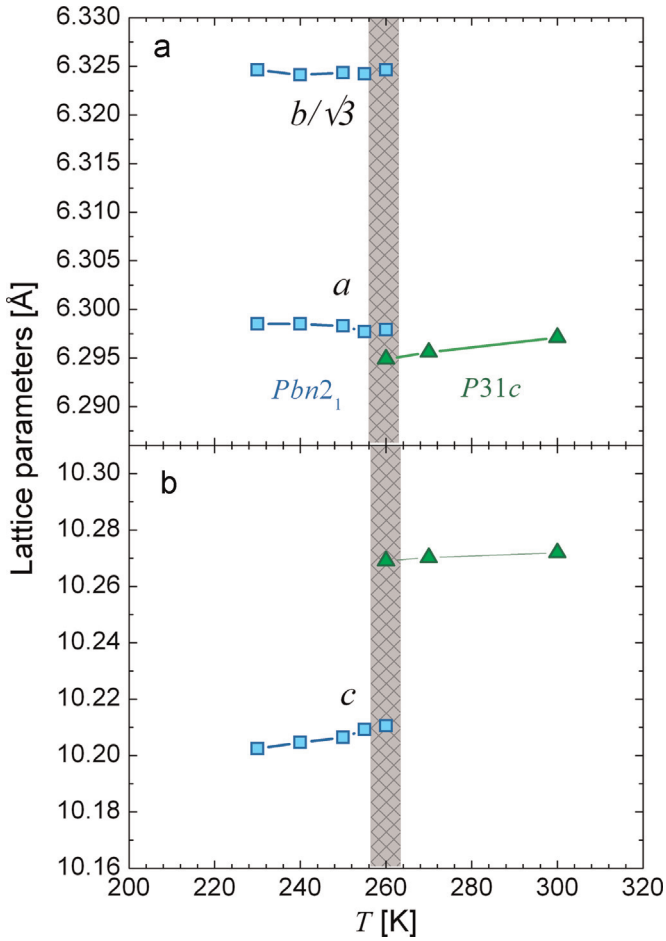


**Fig. 7.** Thermal evolution of lattice parameters $a$ and $b/\sqrt{3}$ (a) and $c$ (b) in the structures $Pbn2_1$ and $P31c$ for a sample $YBaCo_{3.8}Ni_{0.2}O_{7.00}$ (from data collected on cooling). The shadowed region represents the coexistence of phases $Pbn2_1$ and $P31c$.

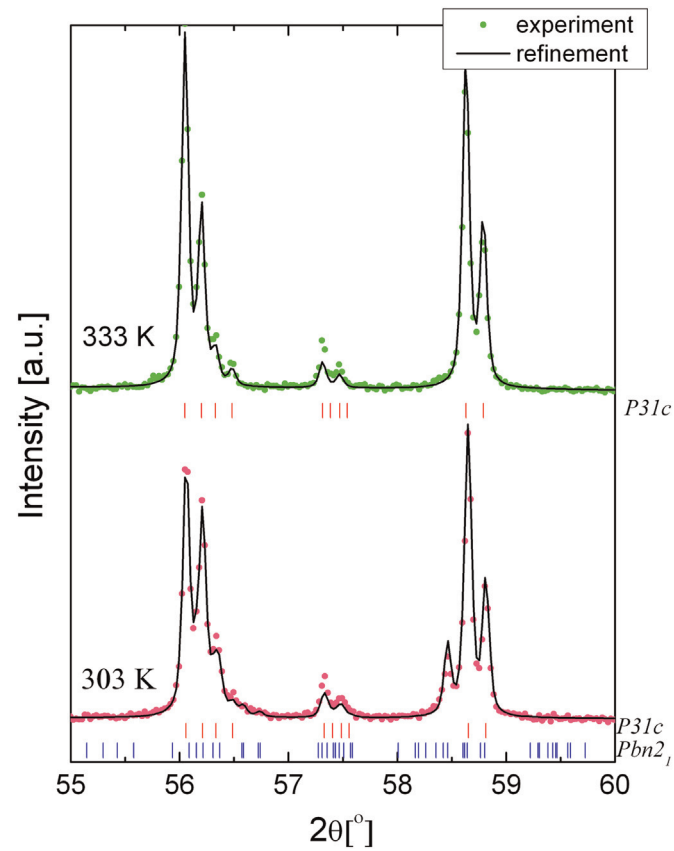


**Fig. 8.** Rietveld refinements (solid lines) for the sample $YBaCo_4O_{7.00}$ at 303 K and 333 K. Symbols correspond to the experimental data collected in a laboratory diffractometer using Cu $K_\alpha$ radiation (only a partial $2\theta$ range is shown). The vertical ticks at the bottom represent the Bragg reflections from the $P31c$ and $Pbn2_1$ space groups.

shrink of the $c$ lattice constant upon cooling has profound implications on the magnetism of the system, as it enhances AFM interactions between Kagomé and triangular cobalt/nickel layers. This issue will be discussed in the following section.

The same analysis was performed in the Ni-20 sample for data collected between 300 K and 250 K on cooling. The lattice parameters are presented in Fig. 7, where we can observe that the structural transition has shifted to lower temperatures, around 260 K. However, doubling the Ni substitution has a negligible effect on the lattice parameters of both phases.

It is interesting to compare these results with the behavior of the parent compound ($x=0$). As mentioned before, although the structure of the $YBaCo_4O_7$ compound has been repeatedly reported in the literature, the fact that at room temperature the transition is not complete when the stoichiometry is truly $\delta=0$ has been overlooked. To resolve this, we performed laboratory XPD both at room temperature and at 330 K. The data at 330 K can be refined nicely to a single-phase in the $P31c$ space group, whereas at 303 K a second $Pbn2_1$ phase accounts for the observed additional reflections. To illustrate this, in Fig. 8 we show a selected region of the Rietveld refinements of the two datasets. Atomic positions were kept fixed at the values refined previously from neutron diffraction data at room temperature on the same sample [22]. The presence of the $Pbn2_1$ phase is confirmed by the additional reflections observed in the 303 K data, which are not detectable at 333 K. In Table 1 we report the obtained lattice parameters for the Ni-0 sample.

**Table 1**
Lattice parameters of the parent compound $YBaCo_4O_{7.00}$ at 303 K and 333 K, obtained from the refinements of XPD data.

| $T$ (K) | $P31c$ | | $Pbn2_1$ | | |
|---|---|---|---|---|---|
| | $a$ (Å) | $c$ (Å) | $a$ (Å) | $b$ (Å) | $c$ (Å) |
| 303 | 6.2972(6) | 10.2727(8) | 6.2991(8) | 10.9506(9) | 10.2247(6) |
| 333 | 6.2995(5) | 10.2736(5) | – | – | – |

In Fig. 9 we show the unit cell volume normalized to one Co atom obtained in the present work for the Ni-0, Ni-10 and Ni-20 samples. For the $Pbn2_1$ phase we also compare with data by Avci et al. [14] who measured lattice parameters above $T_S$, at 313 K. We see in Fig. 9 that the agreement with the present data is excellent, confirming the very little effect on the cell constants of adding Ni at these low doping levels.

### 3.3. Orthorhombic to monoclinic transition

The low-temperature region was explored for the Ni-10 sample using SXPD at LNLS. A longer scan was performed at 10 K in the range $10° < 2\theta < 45°$. We observe evidence of the monoclinic distortion – reported for the parent compound below 110 K – which is indicative of a transition to the $P112_1$ space group driven by the AFM long-range ordering of the system [23]. To track this distortion, short scans were collected around the $(2\ 6\ 0)_O$ Bragg reflection which are shown in Fig. 10. The splitting of the $(2\ 6\ 0)_O$ Bragg reflection into $(2\ 6\ 0)$ and $(\bar{2}\ 6\ 0)$ is very clear from this

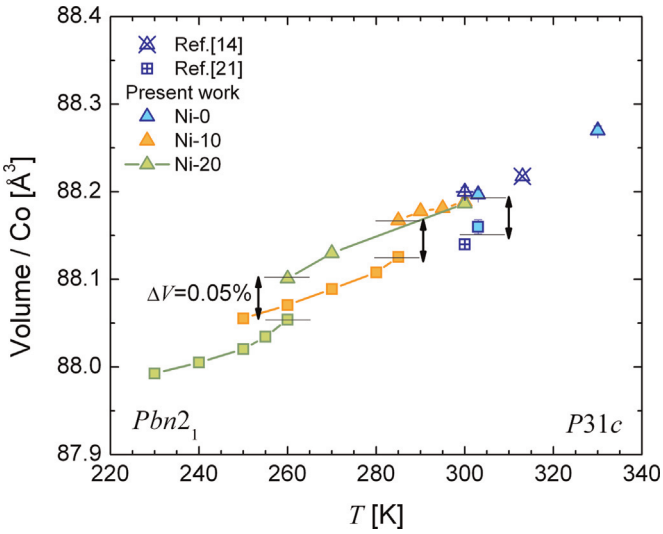


**Fig. 9.** Volume of the unit cell normalized to one Co atom, for samples with $x=0$, $x=0.1$ and $x=0.2$. Triangles represent the trigonal $P31c$ space group, whereas squares represent the orthorhombic $Pbn2_1$. Data from the literature [14] and from our own neutron diffraction results for the parent compound [22] have also been included for comparison.

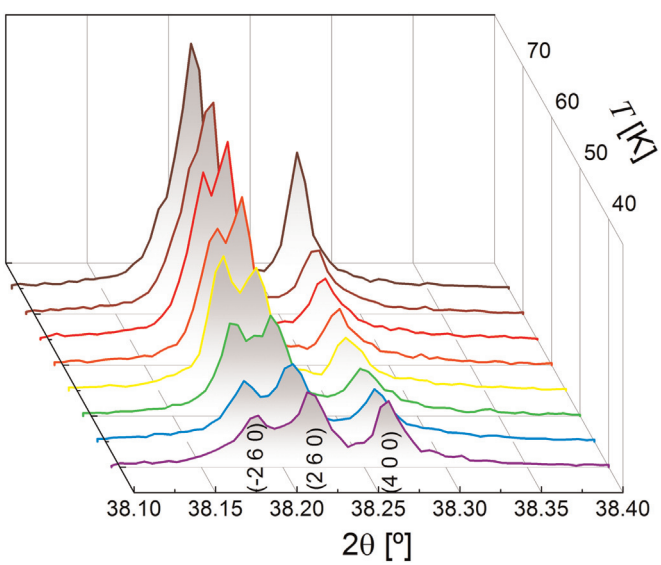


**Fig. 10.** Evolution with temperature of the monoclinic distortion below 100 K in sample $YBaCo_{3.9}Ni_{0.1}O_{7.00}$.

graph. This finding suggests that the samples substituted with Ni could be antiferromagnetically ordered at low temperature just as the parent compound. The lattice parameters $a$ and $c$ in the whole temperature range 10 K < $T$ < 300 K are presented in Fig. 11.

### 3.4. DC-magnetization

In Fig. 12 we present the magnetization ($M$) of the samples in the temperature range 220 < $T$ < 320 K under an applied magnetic field ($H$) of 1000 Oe. The actual values for the magnetization of the Ni-20 sample are higher than for the Ni-0 and Ni-10 samples by a factor of around 2. This discrepancy led us to investigate the possible segregation of a magnetic impurity which could not be detected by the diffraction technique. In Fig. 13(a) we show the magnetization of the samples as a function of $H$ between −10 kOe and 10 kOe at 300 K. It is clear from this figure that the Ni-20 sample has, indeed, a ferromagnetic (FM) contribution to its magnetization at room temperature. Given that this sample was synthesized using metallic Ni as a

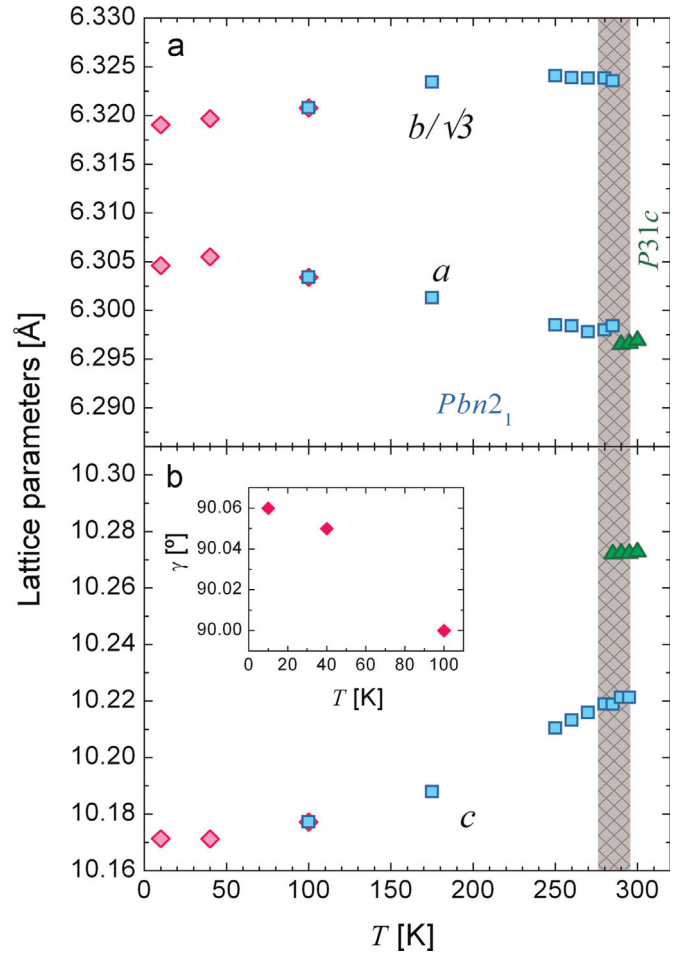


**Fig. 11.** Thermal evolution of lattice parameters $a$, $b/\sqrt{3}$ (a) and $c$ (b) in the whole temperature range from 10 K to 300 K for the sample $YBaCo_{3.9}Ni_{0.1}O_{7.00}$ (data collected on cooling). The inset in (b) shows the refined monoclinic angle $\gamma$ in the $P112_1$ space group.

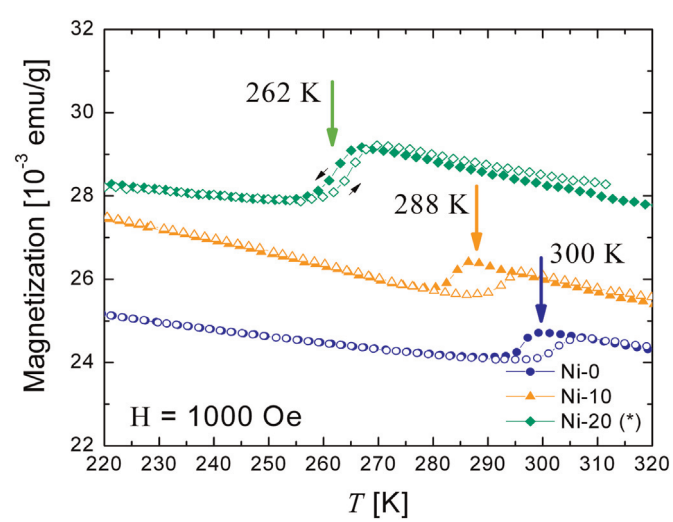


**Fig. 12.** Magnetization as a function of temperature under an applied field of 1000 Oe for samples $YBaCo_4O_{7.00}$, $YBaCo_{3.9}Ni_{0.1}O_{7.00}$ and $YBaCo_{3.8}Ni_{0.2}O_{7.00}$. Solid (empty) symbols correspond to data collected on cooling (warming). The arrows indicate the transition temperatures $T_S$ as the average between the cooling and warming curves at their maximum slope. Curves are vertically shifted for comparison of their $T_S$ values, as we show in Fig. 13(b) that their magnetization should collapse at 300 K.

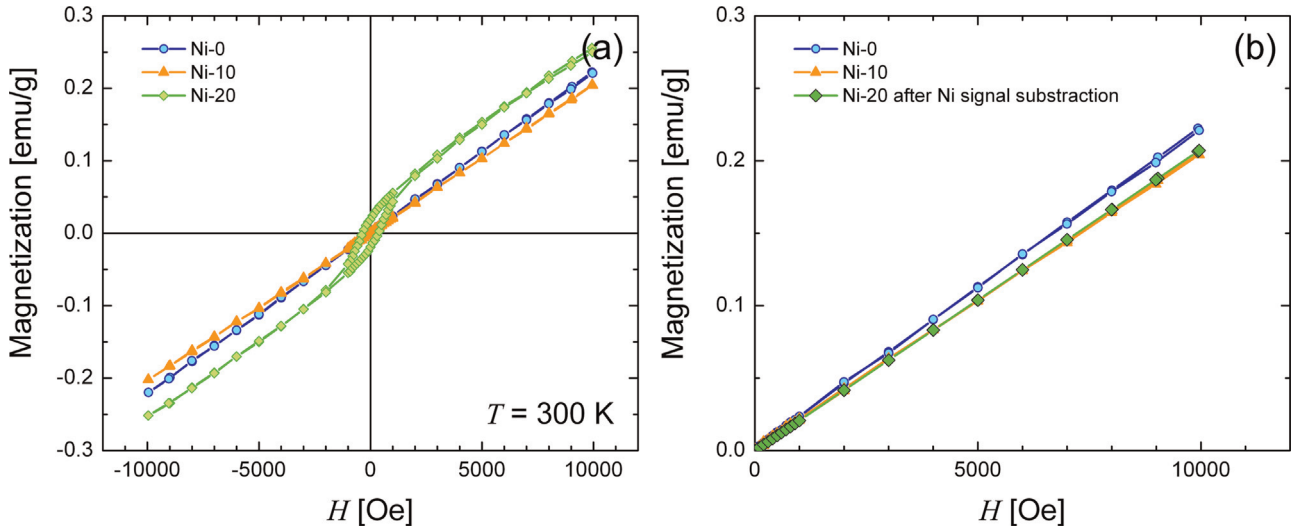


**Fig. 13.** (a) Room temperature magnetization as a function of applied magnetic field, for samples $YBaCo_4O_{7.00}$, $YBaCo_{3.9}Ni_{0.1}O_{7.00}$ and $YBaCo_{3.8}Ni_{0.2}O_{7.00}$. (b) Zoom of first quadrant, in which the magnetization of the Ni-20 sample has been subtracted from the FM signal coming from a small fraction of unreacted metallic Ni.

precursor, a possible hypothesis is that this FM contribution comes from metallic Ni that has not reacted during the synthesis. By considering that such FM Ni is completely saturated above 5000 Oe, the FM signal can be subtracted from the $M$ vs. $H$ curve and quantified, yielding a value of $\approx 0.08$ wt.% metallic Ni (to be compared with the 2 wt.% nominal Ni concentration). The magnetization curve after subtraction of the FM signal is compared in Fig. 13(b) with the ones for samples Ni-0 and Ni-10. We can see that the compound shows a paramagnetic behavior, as expected, and that the room temperature magnetic susceptibility for the two Ni-substituted samples is the same. The Ni-0 sample shows a higher slope, but it should be noted that at 300 K this sample is in the middle of a transition. From the above results we conclude that the solubility limit of Ni in the $YBaCo_{1-x}Ni_xO_{7.00}$ compound lies below $x=0.20$. Once explained why the magnetization of the Ni-20 sample is higher, we compare the curves in Fig. 12 and observe that the three samples reproduce the jump in the magnetization at $T_S$, as had been shown for the parent compound and other members of the family. The sharp orthorhombic distortion of the unit cell at $T_S$ makes it possible for the compound to become ordered below $T_N \approx 100$ K. The jump in the magnetization indicates that below $T_S$ the antiferromagnetic interactions are increased, which can be related to the compression of the cell along the "$c$"-axis bringing closer the Kagomé and triangular sheets of Co atoms.

## 4. Conclusions

In this paper we have studied the structure of samples $YBaCo_4O_{7.00}$ partially substituted with Ni at the Co site. When starting from a metallic Ni precursor, the solubility limit has been found to lie below 5 at.% Ni/Co. This was detected in magnetization measurements which are extremely sensitive to small amounts of ferromagnetic impurities. Although we do not observe any distortion of the crystal lattices upon Ni substitution, the phase stability is strongly modified, as had been shown previously by Maignan et al. [17], shifting the transition temperature up to 40°. Thermodiffraction measurements performed at the synchrotron source of LNLS allowed us to follow the evolution with temperature of the phase stability and lattice constants, which was not reported for the yttrium "114" cobaltite before. We observed a sharp rescaling of the unit cell across the transition $P31c \rightarrow Pbn2_1$ which is strongest along the $c$-direction of the crystal. This contraction is proposed to be responsible for the enhancement of AFM interactions between Co atoms mediated by O, as it brings closer the Kagomé and triangular layers. This manifests in the concomitant drop of the magnetization at $T_S$, which based on a model of a Curie–Weiss paramagnet leads to an increase in $|\theta_{CW}|$, and therefore to the mean-field AFM exchange interactions. It also allows for the development of a long-range AFM order at lower temperatures, not only for the parent compound [9] but also for the Ni-substituted samples [22]. Due to poor grain statistics, a Rietveld refinement of the SXPD data was not possible. Work is in progress using neutron powder diffraction to study the evolution of the inter-atomic distances in the $P31c$ and $Pbn2_1$ phases to confirm this relation. The increased range of stability of the trigonal $P31c$ phase is further evidence of the role played by disorder, which always favors this structure: an oxygen excess completely suppresses the $P31c \rightarrow Pbn2_1$ transition, the substitution at the $R$ site with smaller cations favors the stability of the $P31c$ phase, and we have shown here that also does the substitution at the Co site.

## Acknowledgment

This work is part of a research project supported by Agencia Nacional de Promoción Científica y Tecnológica (Argentina), under grant PICT-2011-0752, by Conicet under grant PIP 490 2012-2014 and by Universidad Nacional de Cuyo. Authors are very grateful to F. Castro at CAB for performing the TGA measurements, and to F. Pomiro for his participation in the preparation of samples. EG acknowledges CNPq and FAPESP for financial support. We acknowledge LNLS synchrotron for the beamtime allocation and financial support. We also thank V. Tognoli and R. Benavides at CAB for their valuable technical support.

## References

[1] M. Valldor, Solid State Sci. 4 (2002) 923.
[2] A.P. Ramirez, Annu. Rev. Mater. Sci. 24 (1994) 453.
[3] C. Lacroix, P. Mendels, F. Mila, Introduction to Frustrated Magnetism: Materials, Experiments, Theory, vol. 164, Springer, Berlin, 2011.
[4] O. Parkkima, H. Yamauchi, M. Karppinen, Chem. Mater. 25 (2013) 599.
[5] O. Parkkima, $YBaCo_4O_{7+\delta}$ and $YMnO_{3+\delta}$ based oxygen-storage materials (Ph. D. thesis), School on Chemical Technology, Aalto University, 2014.
[6] H. Hao, J. Cui, C. Chen, L. Pan, J. Hu, X. Hu, Solid State Ionics 177 (2006) 631.
[7] M. Karppinen, H. Yamauchi, S. Otani, T. Fujita, T. Motohashi, Y.H. Huang, M. Valkeapää, H. Fjellvåg, Chem. Mater. 18 (2006) 490.
[8] T. Motohashi, S. Kadota, H. Fjellvag, M. Karppinen, H. Yamauchi, Mater. Sci.

Eng.: B 148 (2008) 196.
[9] L. Chapon, P. Radaelli, H. Zheng, J. Mitchell, Phys. Rev. B 74 (2006) 172401.
[10] V. Caignaert, A. Maignan, V. Pralong, S. Hebert, D. Pelloquin, Solid State Sci. 8 (2006) 1160.
[11] N. Nakayama, T. Mizota, Y. Ueda, A. Sokolov, A. Vasiliev, J. Magn. Magn. Mater. 300 (2006) 98.
[12] A.I. Rykov, Y. Ueda, M. Isobe, N. Nakayama, Y.T. Pavlyukhin, S.A. Petrov, A. N. Shmakov, V.N. Kriventsov, A.N. Vasiliev, New J. Phys. 12 (2010) 043035.
[13] A. Huq, J. Mitchell, H. Zheng, L. Chapon, P. Radaelli, K. Knight, P. Stephens, J. Solid State Chem. 179 (2006) 1136.
[14] S. Avci, O. Chmaissem, H. Zheng, A. Huq, P. Manuel, J.F. Mitchell, Chem. Mater. 25 (2013) 4188.
[15] T. Sarkar, V. Caignaert, V. Pralong, B. Raveau, Chem. Mater. 22 (2010) 6467.
[16] A. Maignan, V. Caignaert, V. Pralong, D. Pelloquin, S. Hébert, J. Solid State Chem. 181 (2008) 1220.
[17] A. Maignan, S. Hebert, V. Caignaert, V. Pralong, D. Pelloquin, Solid State Commun. 147 (2008) 470.
[18] S. Räsänen, H. Yamauchi, M. Karppinen, Chem. Lett. 37 (2008) 638.
[19] J. Rodríguez-Carvajal, Fullprof: a program for Rietveld refinement and pattern matching analysis, in: Abstracts of the Satellite Meeting on Powder Diffraction of the XV Congress of the IUCr, Toulouse, France, 1990, p. 127.
[20] H. Hao, C. Chen, L. Pan, J. Gao, X. Hu, Physica B: Condens. Matter 387 (2007) 98.
[21] A. Maignan, V. Caignaert, D. Pelloquin, S. Hébert, V. Pralong, J. Hejtmanek, D. Khomskii, Phys. Rev. B 74 (2006) 165110.
[22] L.M. Torre, G. Aurelio, R.D. Sánchez, unpublished work.
[23] D.D. Khalyavin, P. Manuel, B. Ouladdiaf, A. Huq, P.W. Stephens, H. Zheng, J. F. Mitchell, L.C. Chapon, Phys. Rev. B 83 (2011) 094412.